Dispersion requirements in coherent frequency-to-time mapping

Victor Torres-Company,[1,2,*] Daniel E. Leaird,[1] and Andrew M. Weiner[1]

[1]*School of Electrical and Computer Engineering, Purdue University, West Lafayette, Indiana 47907, USA*
[2]*Departament de Física, Universitat Jaume I, 12080 Castelló de la Plana, Spain*
[*]*torres31@purdue.edu*

Abstract: The frequency-to-time mapping technique (also known as the temporal far-field phenomenon) usually requires a significant amount of dispersion to stretch an ultrashort optical pulse so that the intensity profile becomes a scaled replica of its optical spectrum. In this work, we study the near-to-far-field transition and find that the far-field condition can be relaxed in some cases relevant for radio-frequency (RF) waveform generation. This observation has allowed us to achieve intensity signals with an ultrabroad RF bandwidth content.

OCIS codes: (320.7085) Ultrafast information processing; (320.5540) Pulse shaping; (260.2030) Dispersion; (070.2590) ABCD transforms; (060.5625) Radio frequency photonics.

References and links

1. A. M. Weiner, *Ultrafast Optics*, (Wiley Interscience, 2009).
2. V. Torres-Company, J. Lancis, and P. Andrés, "Space-Time analogies in Optics," Prog. Opt. in press).
3. Y. C. Tong, L. Y. Chan, and H. K. Tsang, "Fibre dispersion or pulse spectrum measurement using a sampling oscilloscope," Electron. Lett. **33**(11), 983–985 (1997).
4. M. A. Muriel, J. Azaña, and A. Carballar, "Real-time Fourier transformer based on fiber gratings," Opt. Lett. **24**(1), 1–3 (1999).
5. D. R. Solli, J. Chou, and B. Jalali, "Amplified wavelength-time transformation for real-time spectroscopy," Nat. Photonics **2**(1), 48–51 (2008).
6. M. H. Khan, H. Shen, Y. Xuan, L. Zhao, S. J. Xiao, D. E. Leaird, A. M. Weiner, and M. Qi, "Ultrabroad-bandwidth arbitrary radiofrequency waveform generation with a silicon photonic chip-based spectral shaper," Nat. Photonics **4**(2), 117–122 (2010).
7. S. Moon and D. Y. Kim, "Ultra-high-speed optical coherence tomography with a stretched pulse supercontinuum source," Opt. Express **14**(24), 11575–11584 (2006).
8. M. H. Asghari, Y. Park, and J. Azaña, "Complex-field measurement of ultrafast dynamic optical waveforms based on real-time spectral interferometry," Opt. Express **18**(16), 16526–16538 (2010).
9. S. Thomas, A. Malacarne, F. Fresi, L. Poti, and J. Azaña, "Fiber-based programmable picosecond optical pulse shaper," J. Lightwave Technol. **28**(12), 1832–1843 (2010).
10. K. Goda, K. K. Tsia, and B. Jalali, "Serial time-encoded amplified imaging for real-time observation of fast dynamic phenomena," Nature **458**(7242), 1145–1149 (2009).
11. D. R. Solli, S. Gupta, and B. Jalali, "Optical phase recovery in the dispersive Fourier transformation," Appl. Phys. Lett. **95**(23), 231108 (2009).
12. J. Chou, Y. Han, and B. Jalali, "Adaptive RF-photonic arbitrary waveform generator," IEEE Photon. Technol. Lett. **15**(4), 581–583 (2003).
13. I. S. Lin, J. D. McKinney, and A. M. Weiner, "Photonic synthesis of broadband microwave arbitrary waveforms applicable to ultrawideband communication," IEEE Microw. Wirel. Compon. Lett. **15**(4), 226–228 (2005).
14. J. W. Goodman, *Introduction to Fourier Optics*, 3rd ed., (Roberts and Co. Publishers, 2004).
15. W. L. Stutzman and G. A. Thiele, *Antenna Theory and Design*, 2nd ed., (John Wiley and Sons, 1998).
16. C. Wang, F. Zeng, and J. P. Yao, "All-fiber ultrawideband pulse generation based on spectral-shaping and dispersion-induced frequency-to-time conversion," IEEE Photon. Technol. Lett. **19**(3), 137–139 (2007).
17. M. Abtahi, M. Dastmalchi, S. LaRochelle, and L. A. Rusch, "Generation of arbitrary UWB waveforms by spectral shaping and thermally controlled apodized FBGs," J. Lightwave Technol. **27**(23), 5276–5283 (2009).
18. J. D. McKinney, "Background-free arbitrary waveform generation via polarization pulse shaping," IEEE Photon. Technol. Lett. **22**(16), 1193–1195 (2010).
19. Y. Liu, S. G. Park, and A. M. Weiner, "Enhancement of narrow-band terahertz radiation from photoconducting antennas by optical pulse shaping," Opt. Lett. **21**(21), 1762–1764 (1996).
20. Y. Liu, S. G. Park, and A. M. Weiner, "Terahertz waveform synthesis via optical pulse shaping," IEEE J. Sel. Top. Quantum Electron. **2**, 709–719 (1997).
21. H. N. Chapman and K. A. Nugent, "Coherent lensless X-ray imaging," Nat. Photonics **4**(12), 833–839 (2010).

#154675 - $15.00 USD Received 13 Sep 2011; revised 31 Oct 2011; accepted 31 Oct 2011; published 17 Nov 2011

22. A. M. Weiner, "Femtosecond pulse shaping using spatial light modulators," Rev. Sci. Instrum. **71**(5), 1929–1960 (2000).
23. J. Azaña, L. R. Chen, M. A. Muriel, and P. W. E. Smith, "Experimental demonstration of real-time Fourier transformation using linearly chirped fibre Bragg gratings," Electron. Lett. **35**(25), 2223–2224 (1999).
24. H. Chi, F. Zeng, and J. P. Yao, "Photonic generation of microwave signals based on pulse shaping," IEEE Photon. Technol. Lett. **19**(9), 668–670 (2007).
25. R. E. Saperstein and Y. Fainman, "Information processing with longitudinal spectral decomposition of ultrafast pulses," Appl. Opt. **47**(4), A21–A31 (2008).

1. Introduction

It is very well known that ultrashort optical pulses spread by linear propagation in a dispersive medium due to the fact that each spectral component travels at a different group velocity [1]. The so-called frequency-to-time mapping phenomenon establishes that once sufficient dispersion has been introduced onto the pulse, its temporal profile becomes a scaled replica of the optical spectrum [2–4]. The ability to measure or manipulate the spectral information in the temporal domain has enabled new metrology and signal processing schemes with a superior performance in terms of compactness and operation speed with respect to more conventional approaches. Some of the most recent applications reported that make use of this phenomenon include absorption spectroscopy [5]; radio-frequency arbitrary waveform generation (RF-AWG) [6]; spectral interferometry [7, 8]; rapidly reconfigurable optical pulse shaping [9]; or 2D ultrafast imaging [10], for example.

In order to achieve the correspondence between the optical spectrum and the stretched intensity profile, a minimum dispersion amount must be introduced on the input pulse (the so-called temporal far-field condition [4]). This condition sets a physical limit on the maximum reconfiguration speed in the above mentioned schemes as well as a maximally achievable bandwidth in RF-AWG. Recently, Solli et al. have shown that the spectral information can be alternatively recovered off-line using two temporal intensity measurements in the near-field region [11]. While being a certainly interesting technique for absorption spectroscopy, different applications such as the photonic RF-AWG [12, 13] or temporal Fourier processors [9] require the spectral information mapped to the temporal domain *in situ*. Unfortunately, the temporal far-field or Fraunhofer condition is provided by a strong inequality [4], thus making it challenging to establish the precise amount of dispersion needed in a general case. In this work, we focus on particular waveforms that are interesting for RF photonic applications and study the transition region at which the frequency-to-time mapping is expected to occur. We show that a less restrictive far-field criterion - the "antenna designer's formula" [14, 15] - works well to account for the minimum dispersion amount required to observe the frequency-to-time transformation. This new criterion permits to optimize the design of the RF-AWG based on frequency-to-time mapping [6, 12, 13, 16–18] in terms of maximally achievable bandwidth.

Finally, we provide some examples of waveforms that show the mapping at unexpectedly low dispersion amounts. Although this final observation cannot be generalized to arbitrary waveforms, it has allowed us to obtain intensity signals with ultra-broad bandwidth content that are of significant interest for RF photonic applications and the synthesis of terahertz radiation. We note that with respect to standard techniques for terahertz signal generation based on pulse shaping [19, 20], the frequency-to-time mapping approach relaxes the requirement of the spatial mask because it only requires spectral amplitude modulation.

The remainder of this paper is organized as follows. Section 2 revisits the basic theory for frequency-to-time transformation. We introduce the new criterion and explore its implications in RF-AWG through a relevant numerical example. Section 3 describes the experimental setup employed to study the validity of the new far-field criterion. Section 4 shows three different numerical and experimental results. Finally, Section 5 discusses the main implications of the work before the summary presented in Section 6.

#154675 - $15.00 USD Received 13 Sep 2011; revised 31 Oct 2011; accepted 31 Oct 2011; published 17 Nov 2011

2. Temporal far-field condition revisited

2.1 Theory

Mathematically, the distortion of an ultrashort light pulse in a linear first-order dispersive medium is described by a Fresnel integral [2], i.e.,

$$E_{out}(t) \propto \exp\left(-i\frac{t^2}{2\Phi_2}\right)\int E_{in}(t')\exp\left(-i\frac{t'^2}{2\Phi_2}\right)\exp\left(i\frac{tt'}{\Phi_2}\right)dt'. \qquad (1)$$

Here, as usual, we are referring time with respect to a framework moving with the wavepacket at the group velocity. $E(t)$ represents the complex field envelope of the pulse and Φ_2 the group delay dispersion (GDD) parameter of the medium. We are also taking the definition of Fourier transform of a function $f(t)$ as $F(\omega) \propto \int f(t)\exp(i\omega t)dt$, and the phase factor of a propagating wave-packet $\exp[-i(\omega t - \phi)]$. The desired frequency-to-time mapping occurs when the quadratic phase factor inside the integrand of Eq. (1) is safely discarded. This is achieved when the phase variation within the temporal duration of the input waveform is significantly lesser than a tolerable value. A popular criterion consists of demanding [4]

$$\left|\Phi_2\right| >> \frac{\sigma_0^2}{2\pi}, \qquad (2)$$

where σ_0 is a measurement of the pulse duration of the input field $E_{in}(t)$. From the previous relation, both the strong inequality sign and the ambiguous criterion to define the initial pulse's temporal extension make it very difficult to establish the precise Φ_2 amount for an arbitrary field.

It is interesting to recall that the above problem has a corresponding physical analogue in spatial Fourier optics as the Fraunhofer diffraction, which states that the intensity pattern in the far field of an object is given by the modulus square of the Fourier transform of the aperture field. This is the reason why the frequency-to-time mapping is alternatively referred as the temporal far-field phenomenon [4], and the inequality expressed by (2) is often termed as the far-field criterion. The calculation of the far-field spatial distribution of a radiating source is a well-established problem of technological relevance in fields as diverse as microwave engineering [15] or X-ray optics [21]. It turns out that a less restrictive requirement widely studied for antenna pattern radiation, known as the "antenna designer's formula", works well for many of the problems of interest in spatial Fourier optics [14]. This alternative condition translates into the temporal domain as

$$\left|\Phi_2\right| > \frac{\sigma_0^2}{\pi}. \qquad (3)$$

As first noted in [14], this criterion is less restrictive than (2) because there is only one inequality sign. Mathematically, it implies introducing a phase error of $\pi/8$ in the approximation of the quadratic phase factor by a constant in the integrand of Eq. (1). This inequality is telling us that one does not need to satisfy the far-field inequality (1) by orders of magnitude as one would *a priori* expect, but only twice the minimum amount appears to be sufficient.

2.2 Implications in RF-AWG

We can study the validity of this new criterion through the following analytical example,

$$\tilde{E}_{in}(\omega) = \exp[-\omega^2/2\Delta\omega^2] - \exp[-\omega^2/2\delta\omega^2]. \qquad (4)$$

#154675 - $15.00 USD Received 13 Sep 2011; revised 31 Oct 2011; accepted 31 Oct 2011; published 17 Nov 2011

Here, $\tilde{E}_{in}(\omega)$ represents the complex field envelope of the signal. This function consists of a broad spectral signal of width $\Delta\omega$ on which a spectral feature of width $\delta\omega$ is carved. By calculating the Fourier transform of Eq. (4) and inserting the result in (1), we calculate the intensity profile of the stretched pulse for any dispersion amount as

$$I_{out}(t) = \left|E_{out}(t)\right|^2 \propto \left|g_1(t)\right|^2 + \left|\gamma\right|^2 \left|g_2(t)\right|^2 - 2\left|\gamma\right|\left|g_1(t)g_2(t)\right|\cos\left[(C_1 - C_2)t^2 + \phi\right], \quad (5)$$

where $g_i(t) = \exp\left[-t^2/(2\sigma_i^2)\right]$ with $\sigma_1^2 = 1/\Delta\omega^2 + \Phi_2^2\,\Delta\omega^2$, $\sigma_2^2 = 1/\delta\omega^2 + \Phi_2^2\,\delta\omega^2$, and the chirping values are provided by $C_1 = \Phi_2/\left(1/\Delta\omega^4 + \Phi_2^2\right)$ and $C_2 = \Phi_2/\left(1/\delta\omega^4 + \Phi_2^2\right)$. The coefficient $\gamma = \left[\left(1/\Delta\omega^2 - i\Phi_2\Delta\omega^2\right)/\left(1/\delta\omega^2 - i\Phi_2\delta\omega^2\right)\right]^{1/2}$ and $\phi = \arg[\gamma]$. Equation (5) indicates that the intensity profile is composed by the coherent superposition of two signals with different widths and chirp coefficients. With large dispersion amounts, the chirp coefficients approach $C_i \to 0$ and the factor $\gamma \to 1$. Then the spectral feature gets mapped into the time domain with sufficient visibility and one can safely claim to have entered into the far-zone region. In this example, the temporal extension of the undispersed waveform is inversely proportional to the bandwidth of the spectral feature, $\sigma_0 \sim 1/\upsilon$, where $\upsilon = 1.665\,\delta\omega/(2\pi)$ is the bandwidth defined as the full width at half maximum (FWHM) in Hz. Figure 1(a) plots the achieved intensity profile for $\upsilon = 100$ GHz and a envelope bandwidth $\Delta\omega = 100\delta\omega$, considering the criterion established by Eq. (3) is replaced by an equality sign, i.e., $\Phi_2 = 1/(\pi\upsilon^2)$. As can be observed from Fig. 1(b), this leads to a temporally mapped spectral feature with ~95% visibility. In order to show the independence of this criterion with respect to different spectral widths, Fig. 1(c) shows the required dispersion amount to achieve a 95% visibility for different feature widths and bandwidths, and compares the results with the curve $\Phi_2 = 1/(\pi\upsilon^2)$. As can be seen, there is an excellent match between both trends, indicating that the newly established criterion provided by Eq. (3) can be considered to mark the transition from the near- to the far-field region from a practical perspective. This will be further explored in the next sections through other examples.

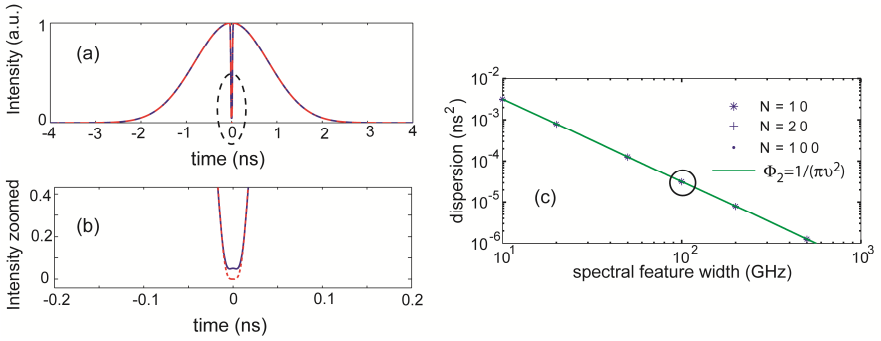

Fig. 1. (a) Intensity profile achieved when $\Phi_2 = 1/(\pi\upsilon^2)$ with $\upsilon = 100$ GHz and $\Delta\omega = 100\delta\omega$ (blue continuous curve) compared with the version of the scaled optical spectrum (red dashed line). (b) Zoomed version of the area highlighted by the dash circle in (a). (c) Dispersion required to achieve a 95% visibility of the dip in the temporal domain for the waveform of Eq. (4) for different spectral feature widths υ. Three different relative optical bandwidths, $N = \Delta\omega/\delta\omega$, are considered. The trend is compared with the minimum amount predicted form Eq. (3) (green continuous line).

#154675 - $15.00 USD Received 13 Sep 2011; revised 31 Oct 2011; accepted 31 Oct 2011; published 17 Nov 2011

The above conclusions have implications of relevance for a photonic-based RF-AWG. Because the duration of the initial waveform is linked to the finest spectral feature with which is shaped by $\sigma_0 \sim 1/\upsilon$, the above criterion allows us to determine the maximally achievable RF bandwidth of the synthesized waveform as the inverse of the shortest temporal feature mapped into time, $\delta t_{\min}$, i.e.,

$$B_{\max} = \frac{1}{\delta t_{\min}} = \frac{1}{\Phi_{2,\min} 2\pi\upsilon} = \frac{\upsilon}{2}. \tag{6}$$

This equation shows that a coarse spectral resolution is more favorable to generate electrical signals with broader bandwidth content.

3. Experimental setup

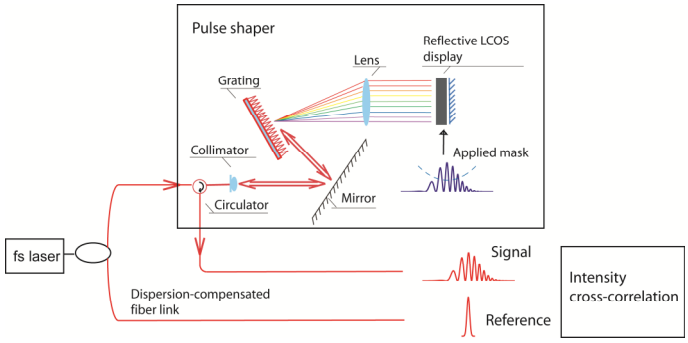

Fig. 2. Schematic representation of the experimental setup. A home-built erbium fiber laser with ~45 nm at full-width at half maximum (FWHM) operating at 53 MHz repetition rate is used as the laser source. The light from the upper arm is shaped with a commercial pulse shaper (Finisar WaveShaper 1000S), that has the capability to manipulate the complex spectrum with 10 GHz resolution in the whole C-band (5 THz bandwidth). It consists of a programmable liquid crystal on silicon display (LCOS) placed at the focal plane of a 4*f* Fourier processor working in a reflective geometry [22]. Finally, the intensity profiles of the shaped pulses are measured by a home-built intensity cross-correlation apparatus working in a non-collinear background-free geometry. In the setup, an achromatic lens focuses the signal and reference beams on a 0.5 mm thick BBO nonlinear crystal to produce second harmonic radiation. The cross-correlator has a motorized mechanical delay stage and it performs the sweep in a few seconds, depending on the temporal duration of the pulse to be measured.

Our aim is to explore the validity of the far-field criterion provided by Eq. (3) in the context of RF-AWG. We synthesize different spectral shapes and measure the achieved intensity profiles after introducing values of known dispersion amounts. The results are compared with the optical spectra properly scaled. For this aim, we have implemented a set up like the one sketched in Fig. 2. The output of a mode-locked femtosecond laser is split in two arms. One beam goes to a Fourier transform pulse shaper. This device has a twofold aim. First, it applies a user-defined spectral mask in order to synthesize the amplitude spectrum to be mapped into the time domain by means of the temporal far-field phenomenon. Secondly, it introduces the required GDD amount in accordance to Eq. (3). In this way, we do not need to replace the dispersive medium for different GDD amounts.

The achieved intensity profiles are measured via intensity cross-correlation, for which the beam propagating through the lower unshaped arm is used as reference. The average powers at the signal and reference arms are −20 dBm and 0 dBm, respectively. The short fiber links connecting signal and reference arms to the cross-correlator are dispersion compensated using carefully selected lengths of dispersion compensating fiber. We note that the pulse shaper truncates slightly the spectrum of the laser. This has the effect of broadening the reference pulse. Overall, we measure a cross-correlation resolution ~260 fs, given by the FWHM of the intensity cross-correlation trace when no amplitude mask is applied on the pulse shaper. This

#154675 - $15.00 USD Received 13 Sep 2011; revised 31 Oct 2011; accepted 31 Oct 2011; published 17 Nov 2011

is close to the limit of 185 fs, estimated by calculating the ideal transform-limited pulses from the measured optical spectra of the signal and reference beams and assuming a flat spectral phase. The discrepancy is attributed to uncompensated third- and higher-order dispersion in the reference beam. Nevertheless, as shall be seen later, this resolution is sufficient to measure the synthesized intensity profiles considering the range of the introduced dispersion amounts.

4. Examples

4.1 The chirped waveform

As can be seen from Fig. 3, the first synthesized waveform is an intensity chirped sinusoidal signal, with a Gaussian envelope width of 2 THz measured at FWHM. This waveform is composed by the coherent superposition of two temporally delayed Gaussian pulses, one that is chirped and another transform limited. Concretely, the synthesized complex spectral envelope is

$$\tilde{E}_{in}(\omega)=\frac{1}{2}\exp\left(-\frac{\omega^2}{2\Delta\omega^2}\right)\left\{\exp\left(i\frac{\Psi}{2}\omega^2\right)\exp\left(-i\omega\tau/2\right)+\exp\left(i\omega\tau/2\right)\right\}, \qquad (7)$$

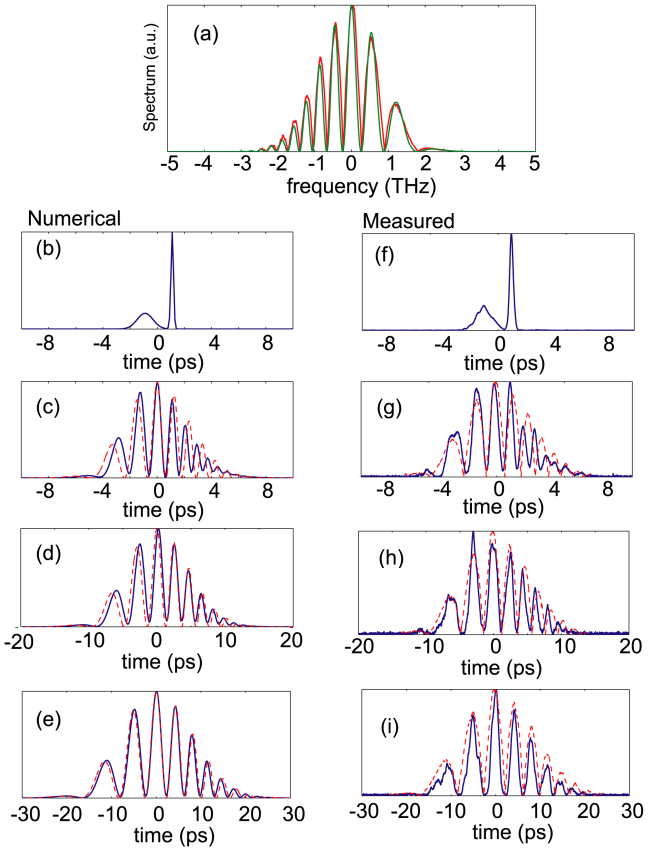

Fig. 3. Chirped waveform: (a) Measured (red) and target (green) optical spectrum. (b)-(e) blue solid line are the numerical intensity profiles at the corresponding GDD amounts of $\Phi_2 = 0; -0.43; -0.86; -1.51\ ps^2$, and red dashed line is the spectrum scaled. (f)-(i) measured intensity profiles at the GDD amount corresponding to the simulated profile on the left column and red-dashed line the scaled measured spectrum.

#154675 - $15.00 USD Received 13 Sep 2011; revised 31 Oct 2011; accepted 31 Oct 2011; published 17 Nov 2011

with the delay $\tau = 2\,ps$ and the chirping coefficient $\psi = 0.108\,\mathrm{ps}^2$. Figure 3(b) illustrates the expected intensity profile for the introduced dispersive amount $\Phi_2 = 0$. Then, taking the temporal extension of this waveform as the separation between pulses, according to Eq. (3), a conservative estimation of the minimum dispersion amount needed to observe the near-to-far-field transition is $|\Phi_{2\min}| = 1.27\,ps^2$. The following plots show how the intensity pattern gets distorted as we introduce higher dispersion amounts in a programmable manner using the pulse shaper. It is interesting to note that for relatively low dispersion amounts, e.g. $|\Phi_2| = 0.43\,ps^2$ in Fig. 3(g), the intensity profile starts to resemble a scaled version of the signal's spectrum. In this case, the loss of visibility for the fastest temporal modulation can be explained by the limited temporal resolution of the measurement. When the GDD amount slightly exceeds the minimum required value, we already observe an excellent match between the spectrum scaled and the measured intensity profile. We note that this value satisfies the inequality given by Eq. (2) only by a factor of ~2.4.

4.2 The cosine profile

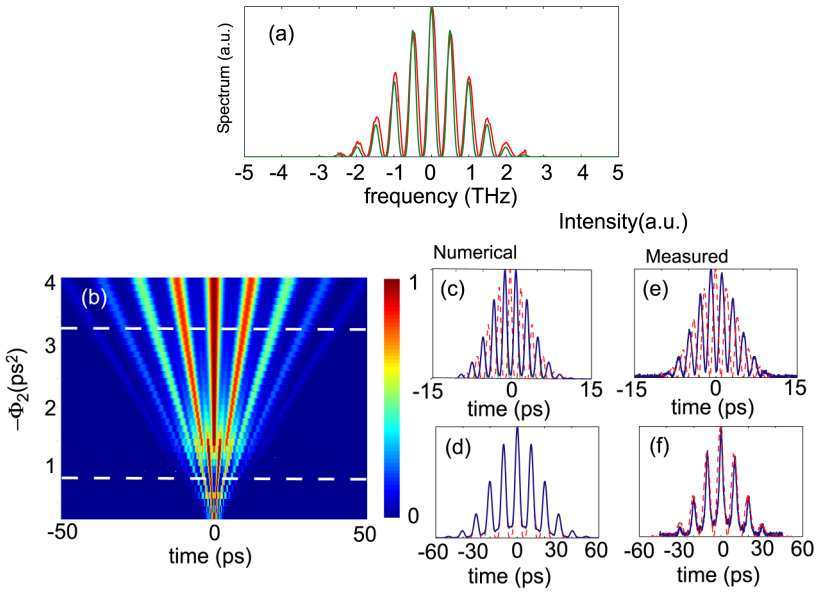

Fig. 4. Cosine profile: (a) Measured (red) and target (green) optical spectrum. (b) Numerically calculated evolution of the intensity profile for different GDD amounts. Simulated intensity profiles (blue line) marked in white dashed line in the 2D plot for (c) $\Phi_2 = -0.65\ ps^2$ and (d) $\Phi_2 = -3.24\ ps^2$. Red dashed line is the spectrum scaled. (e) and (f) measured intensity profiles at the GDD amount corresponding to the same row, and red-dashed line the scaled measured spectrum.

Another interesting example in RF waveform generation is the corresponding to a cosine spectrum, i.e.,

$$\tilde{E}_{in}(\omega) = \frac{1}{2}\exp\left(-\frac{\omega^2}{2\Delta\omega^2}\right)\left\{1+\cos\left(\omega\tau\right)\right\}. \qquad (8)$$

This example is displayed in Fig. 4, which shows the measured and target optical spectrum, for 2 THz bandwidth and synthesized delay of 2 ps. Figure 4(b) illustrates the expected temporal intensity profile for different GDD values. Because the initial profile of this waveform consists of three short pulses separated by 2 ps, a reasonable estimation of the initial duration is 4 ps, thus leading to a minimum required GDD amount of

#154675 - $15.00 USD Received 13 Sep 2011; revised 31 Oct 2011; accepted 31 Oct 2011; published 17 Nov 2011

$\left|\Phi_{2\min}\right| = 5.09\ ps^2$, in accordance to Eq. (3). From Figs. 4(c) and (e), we observe how the signal starts to resemble a scaled version of the synthesized spectrum when the introduced GDD amount ($\Phi_2 = -3.24\ ps^2$) is close to the minimum value required by the antenna's designer criterion. The expected and measured intensity waveforms match closely and resemble a scaled version of the synthesized optical spectrum albeit a slightly reduced visibility.

It is interesting to note that the only significant change in the intensity profile when the dispersion goes from $\Phi_2 = -0.65\ ps^2$ to $-3.24\ ps^2$ is a π phase shift. However, one cannot claim to be in the far-zone region since intermediate dispersions alter the shape of the pulse. However, this observation opens up the question on whether it is also possible to observe the frequency-to-time mapping for other waveforms at significantly lower GDD amounts.

4.3 Two-pulse cosine spectrum

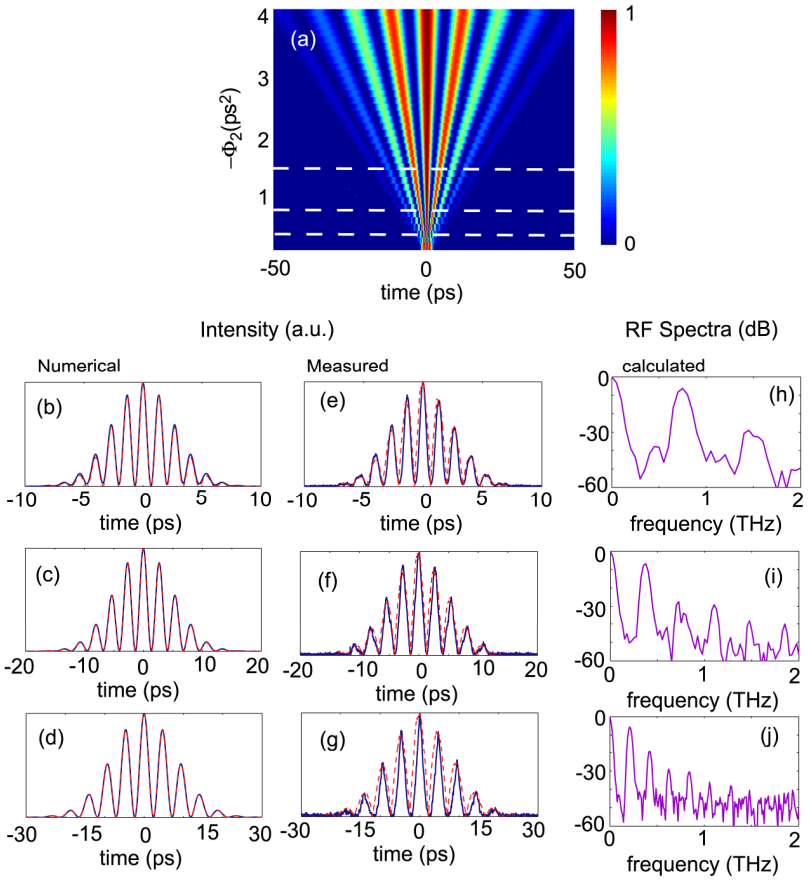

Fig. 5. Two-pulse cosine spectrum: (a) Simulation of intensity profiles for different dispersion amounts. First column shows the simulated intensity profiles (blue line) for the dispersion amounts marked in white dashed line in (a) and compared with the spectrum scaled (red dashed line) for the dispersion amounts (b) $\Phi_2 = -0.43\ ps^2$ (c) $\Phi_2 = -0.86\ ps^2$ (d) $\Phi_2 = -1.51\ ps^2$. (e)-(g) measured intensity profile at the GDD amount corresponding to the same row and red-dashed line the scaled measured spectrum. (h)-(j) calculated RF spectra from the measured intensity profiles at (e)-(g).

The last waveform studied consists of another cosine spectrum,

#154675 - $15.00 USD Received 13 Sep 2011; revised 31 Oct 2011; accepted 31 Oct 2011; published 17 Nov 2011

$$\tilde{E}_{in}(\omega) = \frac{1}{2}\exp\left(-\frac{\omega^2}{2\Delta\omega^2}\right)\left\{\exp\left(i\omega\tau/2\right)+\exp\left(-i\omega\tau/2\right)\right\}, \qquad (9)$$

but now it is only composed of a sequence of two equal amplitude Gaussian pulses with 2 THz FWHM bandwidth separated by $\tau = 2\ ps$. Here, as in the first case, the estimated dispersion amount to observe the frequency-to-time mapping is $|\Phi_2| \geq 1.27\ ps^2$, according to Eq. (3). Figure 5(a) shows the calculated 2D evolution of the intensity profile for different dispersion amounts. It is apparent from this plot that the mapping already takes place at dispersion amounts significantly lower than those predicted by the above rule. To confirm this, we have measured the intensity profiles for different dispersion amounts (those marked with a white dashed line in the 2D plot) and compared them with the numerically calculated ones. As can be seen, for the GDD amount of $\Phi_2 = -0.43\ ps^2$, there is already an excellent correspondence between the achieved intensity profile and the mapped spectrum of the pulse. Now we can claim that the waveform has entered into the far-zone region since by introducing larger dispersion amounts the shape does not change, only its scale, as can be observed from the intensity profiles in Fig. 5(e)-(g). Although the optical spectrum is very similar to the one from the previous example, we note that this waveform is more favorable to achieve the far-field regime with significantly lower dispersion.

This particular waveform is very important for RF photonic applications because, when detected with a high-speed photodiode or a photoconductive antenna with a sufficient bandwidth, it leads to an electrical pulse with the energy concentrated both at dc and at the band centered at $f_0 = \tau/(2\pi|\Phi_2|)$. Thus, noting that it can be generated with dispersion values lower than those predicted by the far-field conditions Eq. (2) or (3) opens the door to synthesize electromagnetic radiation at radically higher frequency bands, including the terahertz domain. We have calculated the corresponding RF spectra for the measured intensity profiles. They are plotted in Figs. 5(h)-(j), which show fundamental RF harmonics peaking at 740 GHz, 370 GHz, and 210 GHz, respectively. In all cases the modulation depth remains very high, as is clearly evident from the intensity cross-correlation traces. This kind of waveform has been extensively studied in the literature [23–25], though generally at lower RF frequencies. The results presented in [24] do show an example of a very high-frequency signal comparable to what is reported here, but with significantly degraded modulation depth. The reduction in modulation depth is likely explained due to the magnitude of the GDD, which is too low to satisfy any of the conditions set forth above. As demonstrated by our results, with the right combination of dispersion and input spectrum, the frequency-to-time mapping paradigm can scale to generation of signals at hundreds of GHz without sacrificing modulation contrast.

The reason why high-fidelity frequency-to-time mapping can take place at low dispersion values in our experiments can be explained as follows. The temporal structure of the pulse when there is no dispersion is composed of a sequence of two Gaussian pulses separated by $\tau = 2\ ps$. As higher dispersion is introduced onto the waveform, the individual pulses spread and start to interfere. This interference pattern becomes a scaled replica of the spectrum of the signal. The key point is that for shorter pulses the dispersion is more notable, and the interference structure appears with high visibility even at amounts significantly lower than those predicted by only taking into account the temporal separation of the pulses (i.e., the initial duration of the waveform). To illustrate this point, we have measured the intensity profile of a sequence of two Gaussian pulses separated by 2 ps at the fixed dispersion of $\Phi_2 = -0.43\ ps^2$ for different values of the bandwidth. The results are shown in Fig. 6. We observe that the frequency-to-time mapping becomes more notable when the bandwidth of the input signal increases. We stress the fact that for the three waveforms, the initial temporal duration (given by the pulse separation) remains fixed. It is clear that not only the temporal duration of the pulse but also its bandwidth content plays a role in the frequency-to-time

#154675 - $15.00 USD Received 13 Sep 2011; revised 31 Oct 2011; accepted 31 Oct 2011; published 17 Nov 2011

mapping conversion. Then, for this waveform, a better estimation of the dispersion amount required to achieve the temporal far field can be provided as follows. We require the duration of the stretched individual pulse to be large enough so that it overlaps with the stretched neighbor pulse, i.e. $\sigma_{0out} > 2\tau$. Then, taking into account that for broadband optical pulses $\sigma_{0out} \approx |\Phi_2| \Delta\omega$, we easily achieve

$$|\Phi_2| > 2\tau/\Delta\omega, \tag{10}$$

i.e., the minimum dispersion grows linearly with the temporal separation of the individual waveforms (instead of quadratically) and inversely with the bandwidth of the constituent pulses. Recalling that the maximum frequency that can be generated is inversely proportional to the GDD amount, the above condition sets an upper limit given by $f_{0,\max} = \tau/(2\pi|\Phi_{2\min}|) = \Delta\omega/(4\pi)$, which, as expected, is only dependent on the available optical bandwidth of the source.

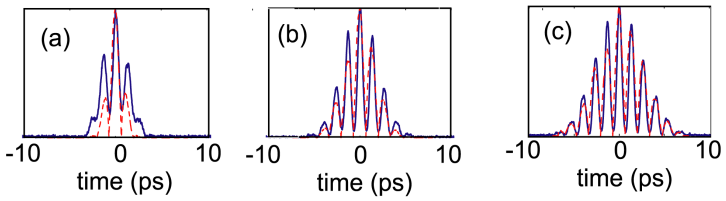

Fig. 6. Two-pulse cosine spectrum: Evolution of the intensity profile at a fixed dispersion amount ($\Phi_2 = -0.43\ ps^2$) and input waveform duration with different bandwidth content. (a) 0.8 THz FWHM bandwidth ; (b) 1.4 THz; and (c) 2.5 THz, leading to visibilities of 69.8%, 90.7% and 94.3%, respectively. Dashed red lines are the corresponding optical spectra scaled.

5. Discussion

The near-to-far-field transition for the last waveform studied clearly benefited from an optical source with broader bandwidth content. One could naturally wonder whether this property is extensible to all waveforms, so that Eq. (10) could be generalized to

$$|\Phi_2| > 2\sigma_0/\Delta\omega, \tag{11}$$

with σ_0 being the temporal duration of the initial waveform. To answer this question, we have calculated numerically the following figure of merit,

$$r_x = 1 - \frac{\int \left[|E_{in}(\omega = t/\Phi_2)|^2 - I_{out}(t) \right]^2 dt}{\sqrt{\int [I_{out}(t)]^2 dt \int |E_{in}(\omega = t/\Phi_2)|^4 dt}}. \tag{12}$$

This parameter quantifies the similarity between the scaled version of the synthesized spectrum of a particular waveform, $|E_{in}(\omega = t/\Phi_2)|^2$, and the intensity profile calculated by propagating it through a linear dispersive medium with GDD coefficient Φ_2, $I_{out}(t)$. The closer the coefficient is to 1, the more similar the waveforms are. We have calculated the minimum dispersion required to achieve a similarity coefficient of 90%, 99% and 99.9% for the four different waveforms, considering different bandwidths, and compared that number with the three different far-field criteria studied in this work. The results are summarized in Table 1.

From Table 1, it is clear that having more optical bandwidth may not always help to get the frequency-to-time mapping at lower dispersions amounts (for instance, the cosine example results are unaffected by having more bandwidth). It is also interesting to note that the

#154675 - $15.00 USD Received 13 Sep 2011; revised 31 Oct 2011; accepted 31 Oct 2011; published 17 Nov 2011

antenna designer's formula has lead to a similarity coefficient >90% for all the studied waveforms. We reiterate that this just implies satisfying Eq. (2) by a factor of 2. Only when inequality Eq. (2) is satisfied by more than an order of magnitude, we can ensure a similarity of >99.9% for all waveforms, which we can interpret as having entered into the far-zone region. With respect to the waveform corresponding to Eq. (4), and from the results in Fig. 1, we observe that requiring 95% of visibility in the temporally mapped feature is more demanding than 99.9% in similarity. We also note that by changing the bandwidth of the input signal, the temporal duration of the chirped waveform changes, and the criteria need to be revised accordingly. Finally, the two-tone cosine represents the only particular example for which neither Eqs. (2) or (3) need to be satisfied in order to get a temporally mapped spectrum with a similarity higher than 99.9% (a number that can be increased with broader optical bandwidth). The criterion given by Eq. (11), which predicts with excellent accuracy the near-to-far field conversion for the two-tone cosine, is much too optimistic for the other waveforms.

Table 1. Comparison of the Accuracy for the Different Far-field Criteria Studied

	Criterion			Φ_2 **required (** ps^2 **)**		
Waveform	*Far-field* Equation (2)	*Antenna* Equation (3)	*Linear* Equation (11)	$r_x = 90\%$	$r_x = 99\%$	$r_x = 99.9\%$
Spectral feature [Eq. (4); $\delta\omega = 0.377$ THz·rad ; $\sigma_0 \sim 10$ ps]						
$\Delta\omega = 3.77$ THz·rad	$\Phi_2 >> 15.9\,\mathrm{ps}^2$	$\Phi_2 > 31.8\,\mathrm{ps}^2$	$\Phi_2 > 5.3\,\mathrm{ps}^2$	.7	12.1	22.7
$\Delta\omega = 7.55$THz·rad	$\Phi_2 >> 15.9\,\mathrm{ps}^2$	$\Phi_2 > 31.8\,\mathrm{ps}^2$	$\Phi_2 > 2.7\,\mathrm{ps}^2$	1.27	4.5	19.4
Chirped [Eq. (7); $\tau = 2\ ps$; $\psi = 0.108\,ps^2$]						
$\Delta\omega = 7.55 THz \cdot rad$; $\sigma_0 \sim 2\ ps$	$\Phi_2 >> 0.64\ ps^2$	$\Phi_2 > 1.27\ ps^2$	$\Phi_2 > 0.53\ ps^2$	0.83	2.6	8.1
$\Delta\omega = 15.1 THz \cdot rad$; $\sigma_0 \sim 4.3\ ps$	$\Phi_2 >> 2.9\ ps^2$	$\Phi_2 > 5.8\ ps^2$	$\Phi_2 > 0.57\ ps^2$	1.69	5.8	18.4
Cosine [Eq. (8); $\tau = 2\ ps$; $\sigma_0 \sim 4$ ps]						
$\Delta\omega = 7.55 THz \cdot rad$	$\Phi_2 >> 2.6\ ps^2$	$\Phi_2 > 5.1\ ps^2$	$\Phi_2 > 1.06\ ps^2$	1.94	3.4	5.6
$\Delta\omega = 15.1 THz \cdot rad$	$\Phi_2 >> 2.6\ ps^2$	$\Phi_2 > 5.1\ ps^2$	$\Phi_2 > 0.53\ ps^2$	1.92	3.4	5.6
Two-tone [Eq. (9); $\tau = 2\ ps$; $\sigma_0 \sim 2\ ps$]						
$\Delta\omega = 7.55 THz \cdot rad$	$\Phi_2 >> 0.64\ ps^2$	$\Phi_2 > 1.27\ ps^2$	$\Phi_2 > 0.53\ ps^2$	0.21	0.36	0.64
$\Delta\omega = 15.1 THz \cdot rad$	$\Phi_2 >> 0.64\ ps^2$	$\Phi_2 > 1.27\ ps^2$	$\Phi_2 > 0.26\ ps^2$	0.10	0.18	0.32

Finally, it is worth contrasting the dispersion requirements for waveform generation with those available from other reports in the literature where the required experimental parameters (dispersion and spectral resolution) are given. We consider a recent work of McKinney [18], where high-quality arbitrary RF waveforms are synthesized through frequency-to-time mapping using a polarization pulse shaping system. Here, the specified spectral resolution is 0.44nm/pixel, which corresponds to an input temporal extension of $\sigma_0 \sim 18.2$ ps . The far-field [Eq. (2)] and antenna designer's formula [Eq. (3)] demand, respectively, $\Phi_2 >> 52.7\,\mathrm{ps}^2$

#154675 - $15.00 USD Received 13 Sep 2011; revised 31 Oct 2011; accepted 31 Oct 2011; published 17 Nov 2011

and $\Phi_2 > 105.4\,\mathrm{ps}^2$. His specified dispersion of ~107 ps^2 is consistent with our finding that is possible to achieve high-fidelity frequency-to-time mapping following the antenna designer's rule.

6. Summary and conclusions

We have studied the temporal far-field or frequency-to-time mapping phenomenon for particular waveforms that are of interest in RF photonic applications. Our goal has been to provide a better estimation of the minimum dispersion required to observe the near-to-far-field transition. In particular, we have shown that the temporal equivalent of the so-called "antenna designer's formula" provides a lesser restrictive estimation than the conventional far-field requirement. This permits to optimize the design of the RF-AWG based on the frequency-to-time mapping in terms of the maximally achievable bandwidth.

In a further step, we have shown two examples that do not need to satisfy any of the above requirements, and achieve the frequency-to-time mapping at significantly lower dispersion amounts. Those particular waveforms concentrate their energy around a high-frequency band inversely proportional to the introduced dispersion amount. Our observations open the door to obtain intensity signals with ultrabroad frequency content approaching the terahertz domain.

Acknowledgments

This project was supported in part by the Naval Postgraduate School under grant N00244-09-1-0068 under the National Security Science and Engineering Faculty Fellowship program. Any opinion, findings, and conclusions or recommendations expressed in this publication are those of the authors and do not necessarily reflect the views of the sponsors. Victor Torres-Company gratefully acknowledges funding from a Marie Curie International Outgoing fellowship (project PIOF-2009-234996).

#154675 - $15.00 USD Received 13 Sep 2011; revised 31 Oct 2011; accepted 31 Oct 2011; published 17 Nov 2011